Geophysical Research Letters

RESEARCH LETTER
10.1029/2024GL110954

Key Points:

- The increase in vapor pressure deficit (VPD) shifts the diurnal peak time of photosynthetic activity to the earlier morning hours
- VPD dominates dryness stress on afternoon photosynthesis depression globally
- CMIP6 ESMs underestimate the negative impact of VPD on afternoon photosynthesis, failing to capture the afternoon depression

Supporting Information:

Supporting Information may be found in the online version of this article.

Correspondence to:

Z. Zhang,
zhaoying_zhang@nju.edu.cn

Citation:

Liu, Y., Peñuelas, J., Cescatti, A., Zhang, Y., & Zhang, Z. (2024). Atmospheric dryness dominates afternoon depression of global terrestrial photosynthesis. *Geophysical Research Letters*, *51*, e2024GL110954. https://doi.org/10.1029/2024GL110954

Received 1 JUL 2024
Accepted 29 NOV 2024

Atmospheric Dryness Dominates Afternoon Depression of Global Terrestrial Photosynthesis

Yue Liu[1,2], Josep Peñuelas[3,4], Alessandro Cescatti[5], Yongguang Zhang[1,2,6], and Zhaoying Zhang[1,2,6]

[1]International Institute for Earth System Sciences, Jiangsu Center for Collaborative Innovation in Geographical Information Resource Development and Application, Nanjing University, Nanjing, China, [2]Jiangsu Provincial Key Laboratory of Geographic Information Science and Technology, Key Laboratory for Land Satellite Remote Sensing Applications of Ministry of Natural Resources, School of Geography and Ocean Science, Nanjing University, Nanjing, China, [3]CSIC, Global Ecology Unit CREAF-CSIC-UAB, Bellaterra, Spain, [4]CREAF, Cerdanyola del Vallès, Spain, [5]European Commission, Joint Research Centre (JRC), Ispra, Italy, [6]International Joint Carbon Neutrality Laboratory, Nanjing University, Nanjing, China

Abstract Satellite observations reveal a widespread afternoon depression of photosynthesis globally. Utilizing satellite observations and eddy covariance tower-based observations worldwide, we investigated the impact of climate factors on the diurnal patterns of ecosystem gross primary production (GPP). Our analysis revealed that the increase in vapor pressure deficit (VPD) shifts the diurnal peak of GPP activity to earlier morning hours, particularly in drylands and areas with short vegetation. After disentangling the strong correlations among VPD, temperature, and soil moisture, we unraveled that VPD emerges as the dominant driver contributing to the widespread afternoon depression of photosynthesis in terrestrial vegetation globally. However, Earth System Models (ESMs) systematically underestimate the significant role of VPD in regulating photosynthesis. Eight out of 10 ESMs exhibited a clear afternoon increase in photosynthesis, which was attributed to temperature. Our findings emphasize the need to enhance the negative effects of VPD on diurnal photosynthesis in ESMs.

Plain Language Summary Diurnal variations in gross primary production (GPP) provide crucial insights into vegetation's response to climate factors. Satellite observations reveal a widespread afternoon depression in photosynthesis. We studied the impact of climate factors on diurnal GPP patterns using satellite and flux tower data. We found that the increase in vapor pressure deficit (VPD) shifts the diurnal peak of GPP to earlier morning hours, particularly in drylands and regions with short vegetation. After disentangling the interactions between VPD, air temperature, and soil moisture, VPD emerges as the primary driver of the afternoon depression of photosynthesis. However, Earth System Models (ESMs) often underestimate VPD's role in regulating photosynthesis, showing an afternoon increase in photosynthesis driven by temperature in most regions. Our findings highlight the need to improve ESMs by incorporating the negative effects of VPD on diurnal photosynthesis.

1. Introduction

Terrestrial gross primary productivity (GPP) constitutes a significant component of the CO_2 flux in global ecosystem carbon exchange (Beer et al., 2010). Understanding the large-scale diurnal dynamics of GPP is vital for accurate carbon budget estimates under climate change. GPP demonstrates marked diurnal variations driven by changes in environmental factors, including solar radiation, temperature, and water availability (Lin et al., 2019). As climate change progresses, changes in environmental conditions may influence the timing and magnitude of the GPP peak throughout the day (Zhang et al., 2018). Solar radiation tends to peak at local solar noon, whereas VPD typically peaks in the afternoon due to its close dependence on air temperature (Wilson et al., 2003). In fact, VPD is influenced by both air moisture content and temperature, increasing significantly with rising temperatures and decreasing air moisture content (Will et al., 2013). Higher values of afternoon VPD induce stomatal closure to reduce transpiration, significantly impacting the diurnal cycle of carbon assimilation (Lin et al., 2019). Elevated temperatures can boost photosynthetic rates in the early morning, but may induce midday declines in GPP due to heat stress (Wilson et al., 2003). The diurnal variation of GPP is also closely linked to soil moisture availability, with GPP peaking earlier as soil moisture decreases, particularly during the dry season when precipitation is

10.1029/2024GL110954

limited (Bucci et al., 2019; Khan et al., 2022). Therefore, understanding how these alterations affect the large-scale diurnal patterns of GPP is increasingly crucial for accurate predictions of the carbon cycle.

The impact of climate change on large-scale GPP at intermediate to long time scales has been extensively studied using polar-orbiting satellites such as Landsat, MODIS, and OCO-2 (Irons et al., 2012; Sun et al., 2017; Zhang et al., 2017). However, climate factors become less explanatory at long time scales due to the pronounced influence of plant phenology, climatic conditions and nutrient availability on photosynthetic seasonality (Wu et al., 2017). The primary climatic drivers of GPP variation may change across seasons (Chen et al., 2024). Additionally, temperature and soil moisture have slow and cumulative effects on plant phenology (Ding et al., 2020). On sub-daily timescales, climatic factors have a more immediate and pronounced influence on photosynthesis than on seasonal scales, with plant physiological processes responding more rapidly to water and heat stress than to changes in canopy structure (Wu et al., 2017). Plant stomata show an almost instantaneous response to light and VPD to optimize water use, whereas the vegetation structure barely changes within a day (Zhang et al., 2024). In fact, diurnal variations in GPP reflect the regulation of land-atmosphere interactions through physiological and environmental controls (Xiao et al., 2021; Zhang et al., 2024), emphasizing vegetation is physiological responses to key environmental drivers. Understanding the key drivers of large-scale diurnal GPP variation is crucial for revealing the physiological regulation of carbon-water fluxes and their associated climate feedbacks.

Emerging satellite observations, such as those from the Orbiting Carbon Observatory-3 (OCO-3), provide unprecedented opportunities to study diurnal variations in large-scale vegetation photosynthesis and their responses to environmental conditions. In this study, we utilize satellite observation-based OCO-3 solar-induced chlorophyll fluorescence (SIF) data sets, global sub-daily GPP_{SIF} data sets (Zhang, Guanter, et al., 2023), and half-hourly GPP fluxes from FLUXNET sites to explore the diurnal dynamics of photosynthesis and identify the primary climatic drivers that control its variability. We disentangle the strong correlations among VPD, air temperature (T_{air}), and soil moisture (SM), subsequently unraveling their individual impacts on constraining the global afternoon depression of photosynthesis. Additionally, we explore the diurnal pattern of GPP simulated by Earth system models (ESMs) to understand the primary factors governing its diurnal variations in the model world.

2. Materials and Methods

2.1. Satellite SIF Data Set

We used OCO-3 SIF (v10) from NASA GES DISC to investigate the diurnal patterns of global SIF (Taylor et al., 2020). OCO-3 SIF is observed at different times of the day within multi-day windows due to the orbital characteristics of the International Space Station (ISS) (Taylor et al., 2020). We used only the 757 nm SIF due to its stronger signal (Zhang et al., 2020). We constructed the global diurnal pattern of SIF using all available observations from August 2019 to July 2023.

We used the global sub-daily (hourly) GPP_{SIF} data generated by Zhang, Guanter, et al. (2023) to examine the effects of climate factors on the diurnal patterns of ecosystem photosynthesis. This data set uses artificial neural networks to generate SIF of spatiotemporally continuous monthly averaged circadian cycles based on OCO-3 and further predict monthly average hourly GPP at 0.5° grid resolution from 2000 to 2021 (Zhang, Guanter, et al., 2023). We derived the time of peak GPP hour, the diurnal centroid of GPP (C_{GPP}), and the ratio of afternoon GPP to morning GPP (ΔGPP) as indicators of the physiological stress of diurnal variation in vegetation. These diurnal metrics adequately describe the diurnal pattern (symmetry or asymmetry) of GPP (Li et al., 2023). ΔGPP indicates the relative difference between the average GPP in the afternoon (12:00–18:00) and that in the morning (6:00–12:00) (Equation 1). This normalization allows for comparisons across different times of the year and GPP levels.

$$\Delta \text{GPP} = \frac{\text{GPP}_{\text{AM}} - \text{GPP}_{\text{PM}}}{\text{GPP}_{\text{AM}}} \times 100\% \tag{1}$$

The diurnal centroid is often used to quantify the diurnal shifts in EC flux variables induced by environmental conditions (Khan et al., 2022). C_{GPP} was calculated using Equation 2:

$$C_{\text{GPP}} = \frac{\sum(\text{GPP}_t \times t)}{\sum \text{GPP}_t} \times 100\% \tag{2}$$

where t is the time in decimal hours from 6:00 to 18:00 (6:00 a.m. to 6:00 p.m.) and GPP_t is the GPP at hour t. The resulting C_{GPP} is the weighted mean hour of the diurnal cycle of GPP. If the variable GPP_t is perfectly symmetrical about local noon, then C_{GPP} would be 12 hr (local noon). If the C_{GPP} is greater than 12, it indicates a shift of the GPP peak time toward the afternoon, while if the C_{GPP} is less than 12, it indicates a shift toward the morning.

2.2. Eddy Flux Data

For comparison with satellite observations, we used the half-hourly GPP from the FLUXNET2015 data set (Pastorello et al., 2020). We used the GPP estimates from the night-time partitioning method for the analysis (GPP_NT_VUT_REF). The final selection comprises 72 flux sites distributed across the globe. This data processing pipeline and site information are detailed in Text S1 and Table S1 in Supporting Information S1. Similarly, for each site, half-hourly GPP data were averaged to two daily values, one each for the morning and afternoon, and $\Delta\text{GPP}_{\text{EC}}$ was calculated using Equation 1.

2.3. Climate and Vegetation Data Sets

We obtained the monthly average hourly data for 2-m T_{air}, dew point temperature (T_{dew}), SM, and short-wave radiation from the fifth European Center for Medium Range Weather Forecasting (ECMWF) ReAnalysis (ERA5) with a spatial resolution of 0.25°. Here, SM was 0–100 cm volumetric SM, with a weighted average from three levels of SM (0–7 cm, 7–28 cm, and 28–100 cm) according to their respective depths. T_{air} and T_{dew} were used to calculate VPD using the equation described in a previous study (Hersbach et al., 2020). All data sets were aggregated to a spatial resolution of 0.5°.

The aridity index is defined as the ratio of precipitation to potential evapotranspiration. We used precipitation and potential evapotranspiration data from the Climate Research Unit v4.06, from 1990 to 2021, with a spatial resolution of 0.5° (Harris et al., 2020). The classifications included hyper-arid ($\text{AI} < 0.05$), arid ($0.05 \le \text{AI} < 0.2$), semi-arid ($0.2 \le \text{AI} < 0.5$), sub-humid ($0.5 \le \text{AI} < 0.75$), humid ($0.75 \le \text{AI} < 1.2$), and hyper-humid ($\text{AI} \ge 1.2$) subtypes. We used the MODIS land cover type (MCD12Q1) version 6.1 data product, with a spatial resolution of 500m (Friedl et al., 2010). We used the GLOBMAP Leaf Area Index (LAI) version 3.0 data with 8-day temporal and ~0.07° spatial resolution (Liu et al., 2012).

2.4. Decoupling Analysis

Following previous studies (Liu et al., 2020), we discretized the data into 10 bins based on percentile values of VPD, T_{air}, and SM per pixel. These bins were used to factor out the impact of VPD and T_{air} or SM on afternoon depression, by assessing the response of ΔGPP at changes to one of the drivers while keeping the other driver constant. The changes in ΔGPP from low VPD to high VPD without T_{air}-VPD coupling (termed ΔGPP (VPD|T_{air})) can quantify the VPD stress on ΔGPP. The specific method was presented in Text S2 and Figure S1 in Supporting Information S1. We evaluated the relative role of VPD, T_{air}, and SM on ΔGPP: ΔGPP (VPD|T_{air}), ΔGPP (T_{air}|VPD), ΔGPP (VPD|SM), and ΔGPP(SM|VPD).

Additionally, to enhance the robustness of our results, we utilized a random forest (RF) model to analyze the sensitivity of ΔGPP to VPD, T_{air}, SM, solar radiation and LAI, as detailed in Text S3 in Supporting Information S1.

2.5. CMIP6 ESMs Simulations

Outputs from 10 ESMs contributing to CMIP6 were analyzed (Table S2 in Supporting Information S1). These CMIP6 models include CMCC-CM2-SR5, CMCC-ESM2, CNRM-CM6-1, CNRM-ESM2-1, HadGEM3-GC31-LL, IPSL-CM6A-LR, IPSL-CM6A-LR-INCA, KIOST-ESM, NorESM2-LM and NorESM2-MM. The simulation of GPP is driven by the dynamics of soil moisture, energy balance, permafrost thawing, atmospheric CO_2 fertilization, nitrogen limitations, and land use change. In this study, historical 3-hr GPP (2010–2014) from each CMIP6 model was resampled to hourly temporal resolution using linear interpolation, which preserves temporal continuity and ensures reliable comparisons. Similarly, hourly GPP data were averaged to two daily values, one each for the morning and afternoon, and ΔGPP_{CMIP6} was calculated using Equation 1. Then, we examined the spatial patterns of ΔGPP_{CMIP6} for 10 models and investigated the factors driving the diurnal variations in GPP.

3. Results

3.1. Diurnal Patterns and Climatic Factors Influences on Global Photosynthesis

For most terrestrial vegetation globally, GPP was slightly higher in the morning than in the afternoon, indicating a widespread afternoon depression (OCO-3 SIF: 70.7%; GPP_{SIF}: 98.9%) (Figure S2 in Supporting Information S1). The afternoon depression of photosynthesis was further confirmed by GPP measurements from flux towers (Figure S3 in Supporting Information S1). The afternoon depression of photosynthesis can be observed by the difference between afternoon and morning GPP ($\Delta GPP = (GPP_{AM}–GPP_{PM}) \times 100\%/GPP_{AM}$). We investigated the role of heat stress and dryness in the afternoon depression of GPP at global and pixel levels. The VPD and temperature showed strong positive relationships with ΔGPP_{SIF} in nearly 83% of the terrestrial regions, exhibiting high correlations in western North America, central South America, tropical areas, and southern Africa (Figures 1a and 1d), suggesting that the increase in heat and atmospheric dryness contributed to the intensification of the afternoon depression. In contrast, an increase in soil moisture was beneficial for mitigating afternoon depression (Figure 1g). At the pixel level (Figures 1b, 1e and 1h), ΔGPP_{SIF} exhibited the strongest positive correlation with VPD ($r = 0.61$, $p < 0.001$), followed by temperature ($r = 0.45$, $p < 0.001$), and showed a sharp increase with temperature above 26°C. ΔGPP_{SIF} displayed a comparatively lower negative correlation with soil moisture ($r = -0.22$, $p < 0.001$).

The diurnal centroid of GPP (C_{GPP}) serves as an indicator of whether the GPP peak time activity tends toward the morning or afternoon. We observed that C_{GPP} exhibited the strongest negative correlation with VPD ($r = -0.6$, $p < 0.001$), showing a noticeable shift toward earlier morning times, from around 12:00 noon to 10:30 a.m. as VPD increased (Figure 1c). The correlation coefficient between C_{GPP} and temperature was −0.56 ($p < 0.001$). C_{GPP} showed minimal variation with temperature until it reached 26°C (around 12:00 noon), beyond which it significantly decreased (from 12:00 noon to 10:30 a.m.) (Figure 1f). The annual average diurnal variations of GPP under different climatic conditions revealed that the afternoon depression of GPP intensified as the VPD gradient increased, accompanied by a notable shift in the GPP peak time toward the earlier morning hours (Figure 1j). No significant shifts in the GPP peak hour or ΔGPP were observed across temperature and soil moisture gradients (Figures 1k and 1l). Furthermore, correlation analyses showed the relationship between ΔGPP_{SIF} (C_{GPP}) and VPD or temperature strengthened as the aridity index decreased (i.e., toward more drought conditions) (Figure S4 and Figure S5 in Supporting Information S1). We also found that the GPP peak occurred earlier in dry environments (semi-arid, arid, and hyper-arid zones) than in humid zones, and the peak shifted further toward earlier morning times with increasing soil moisture limitation (Figure S6 in Supporting Information S1), with VPD identified as the primary driver of this phenomenon (Figure S7 in Supporting Information S1).

3.2. Independent Effects of Climatic Drivers on Photosynthesis Afternoon Depression

We decoupled VPD and temperature using a binned decoupling approach and demonstrated that elevated VPD notably enhanced ΔGPP_{SIF} at relatively higher temperature levels, while it did not markedly change ΔGPP_{SIF} at low temperature levels due to concurrently low VPD (Figure 2a). In contrast, ΔGPP_{SIF} increased significantly with rising temperature only at low VPD levels, and no longer increased, remaining stable when temperature reached its middle percentiles (>40th percentile) (Figure 2b). The respective effects of temperature and VPD on the ΔGPP_{SIF} are illustrated in Figure 2c. The changes in ΔGPP_{SIF} from low VPD to high VPD at the same temperature bin (termed ΔGPP_{SIF} ($VPD|T_{air}$)) can quantify the VPD stress on ΔGPP_{SIF}. Both satellite (Figure 2d) and site observations (Figure S8d in Supporting Information S1) showed that the high VPD effect was strong (ΔGPP_{SIF} ($VPD|T_{air}$) = 2.44%, ΔGPP_{EC} ($VPD|T_{air}$) = 3.43%), in contrast to the high temperature effect (ΔGPP_{SIF} ($T_{air}|VPD$) = 1.74%, ΔGPP_{EC} ($T_{air}|VPD$) = 2.89%).

Spatially, we found that ΔGPP_{SIF} ($VPD|T_{air}$) was positive across 60.2% of vegetated areas (Figure 2e). High ΔGPP_{SIF} ($VPD|T_{air}$) values were observed in the tropics and mid-to low latitudes, including South America, Africa, South Asia, and northern Australia. Conversely, ΔGPP_{SIF} ($T_{air}|VPD$) was smaller in most regions, and it was slightly higher than ΔGPP_{SIF} ($VPD|T_{air}$) in high-latitude regions, which was also visible along the latitudinal gradient (Figures 2e and 2f). High VPD limitation effects were strongest in semi-arid and semi-humid regions,

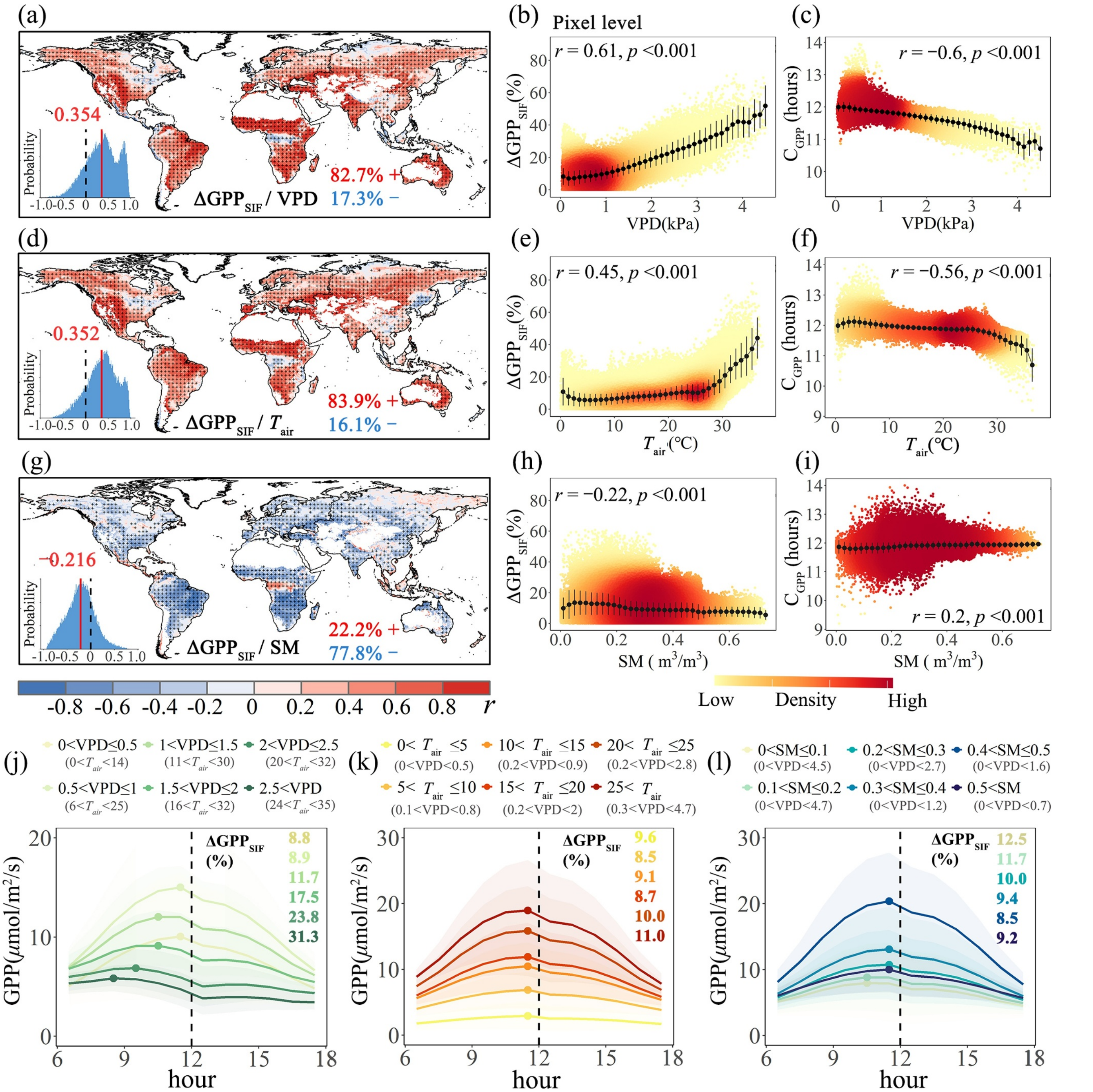

Figure 1. Relationship between diurnal metrics and climatic factors from 2000 to 2021. (a, d, g) Spatial distribution of Pearson's correlation coefficient between monthly average ΔGPP_{SIF} ($\Delta GPP_{SIF} = (GPP_{AM} - GPP_{PM})$ 100%/GPP_{AM}) and monthly VPD (or T_{air}, SM). (b, e, h) Relationships between monthly average ΔGPP_{SIF} and monthly VPD (or T_{air}, SM) at the pixel scale. (c, f, i) Relationships between monthly average diurnal centroid (C_{GPP}) and monthly VPD (or T_{air}, SM) at the pixel scale. (j–l) Annual average diurnal variations in GPP across different climatic factor gradients. T_{air} range for each VPD bin in parentheses of the legend in (j). VPD range for each T_{air} or SM bin (k,l). The kernel density distributions of the correlation coefficients between ΔGPP_{SIF} and VPD (or T_{air}, SM) are shown in the lower-left corner of each panel. The red vertical lines and numbers represent the medians. The numbers in the bottom right corner of each map panel represent the area percentages of positive (+, red) and negative (−, blue) correlations. The regions labeled with black dots indicate significant trends ($p < 0.05$).

including savannas, woody savannas, croplands, and grasslands (Figure 2g). In hyper-arid and hyper-humid regions, afternoon GPP was more stressed by high temperature than by VPD, while the high VPD effect was stronger in other regions (Figures 2g and 2h).

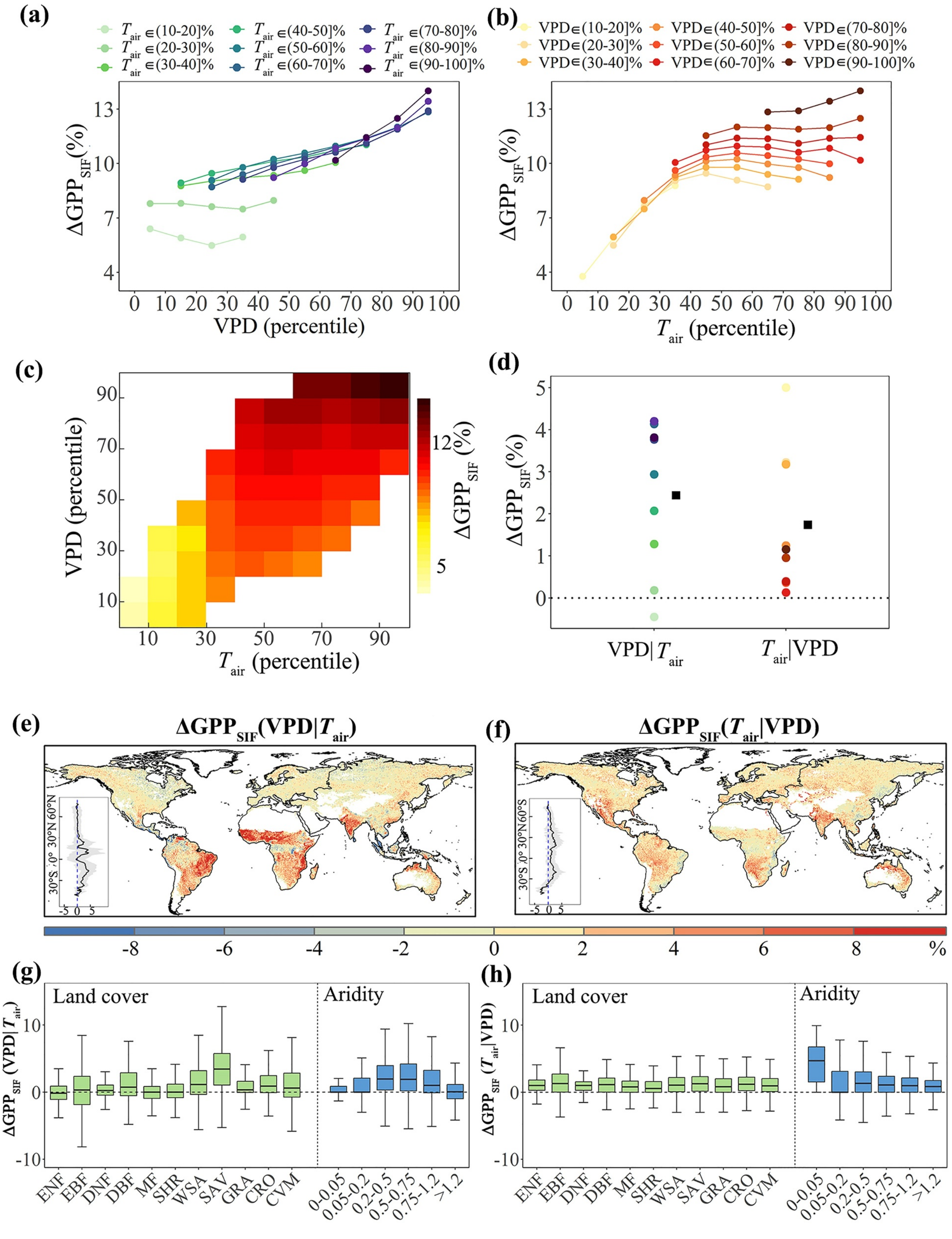
(a)
ΔGPP_SIF(%)
VPD (percentile)
(b)
T_air (percentile)
(c)
VPD (percentile)
T_air (percentile)
(d)
VPD|T_air
T_air|VPD
(e)
ΔGPP_SIF(VPD|T_air)
(f)
ΔGPP_SIF(T_air|VPD)
(g)
Land cover
Aridity
ENF
EBF
DNF
DBF
MF
SHR
WSA
SAV
GRA
CRO
CVM
0-0.05
0.05-0.2
0.2-0.5
0.5-0.75
0.75-1.2
>1.2
(h)
Land cover
Aridity

Figure 2.

Our observations of ΔGPP responses to distinct VPD–SM regimes at satellite and flux towers consistently indicated that afternoon depression of GPP was more pronounced under higher VPD conditions, regardless of soil moisture (Figures S9 and S10 in Supporting Information S1). In contrast, low soil moisture had a limited effect on $\Delta GPP_{SIF.}$ The high VPD effect was strong (ΔGPP_{SIF} (VPD|SM) = 3.70%), compared to the low soil moisture effect (ΔGPP_{SIF} (SM|VPD) = 1.17%). Spatially, VPD showed a more pronounced influence on the afternoon depression of GPP, while ΔGPP_{SIF} (SM|VPD) was small and close to zero across large areas. The limiting effect of low soil moisture exceeded that of high VPD only in northern South America and African woody savannas (Figure S9e and S9f in Supporting Information S1).

We also analyzed the sensitivities of ΔGPP to VPD, temperature, soil moisture, solar radiation and LAI using RF models. VPD emerged as the most critical factor driving the diurnal asymmetry of GPP, followed by temperature, soil moisture, solar radiation and LAI (Figure S11 in Supporting Information S1). Arid regions were most sensitive to variations in atmospheric dryness, while Northern Hemisphere alpine regions showed strong sensitivity to temperature, and wet areas, such as northern South America, exhibited strong responses to soil moisture variability. Radiation showed positive sensitivity in the Southern Hemisphere and negative sensitivity at high northern latitudes. In contrast, ΔGPP was less sensitive to LAI. Both EC flux towers and satellite observations demonstrated that the afternoon depression of GPP was most sensitive to VPD.

3.3. Comparison With CMIP6 ESMs Simulations

We assessed the independent effects of VPD, temperature and soil moisture on afternoon depression of GPP from 10 CMIP6 ESMs. Among 10 CMIP6 models, only CMCC-CM2-SR5 and CMCC-ESM2 displayed widespread afternoon depression over 72.2% of global areas. The remaining models failed to identify afternoon depression and, on the contrary, showed extensive afternoon enhancement of GPP in 60.4%–92.3% of terrestrial ecosystems (Figure S12 in Supporting Information S1). None of the ESMs captured the negative effects of VPD on afternoon GPP (Figure 3). Specifically, without temperature-VPD coupling, CMCC-CM2-SR5 and CMCC-ESM2 identified temperature as the primary factor driver of the afternoon depression (Figures 3a and 3b). In different vegetation types, the afternoon depression induced by high temperature generally exceeded the limiting effects of high VPD, particularly in mixed forests and deciduous broadleaf forests (Figure S13 in Supporting Information S1). Other models showed that while ΔGPP increased significantly with temperature, GPP exhibited afternoon enhancement (ΔGPP <0) at moderate temperature and VPD levels. Out of 10 ESMs, only KIOST-ESM (Figure 3h) indicated that the relative effect of high VPD was greater than that of high temperature, but it still underestimated high VPD stress effects, resulting in a widespread afternoon GPP enhancement. NorESM2-LM, NorESM2-MM, CMCC-CM2-SR5, and CMCC-ESM2 all use the Community Land Model, while NorESM2-LM and NorESM2-MM showed that increased VPD slightly enhanced afternoon GPP (Figures 3i and 3j). These imply that the ESMs may not accurately simulate the GPP response to environmental factors. Additionally, without SM-VPD coupling, all the ESMs showed that ΔGPP increased significantly with increasing VPD, while soil moisture had no significant effect on ΔGPP (Figures 3k–3t). Nonetheless, GPP still exhibited afternoon enhancement at moderate levels of soil moisture and VPD. In conclusion, all ESMs underestimated the negative impact of increasing VPD (especially at high VPD) on afternoon photosynthesis and likely overestimated the stress resistance of afternoon photosynthesis.

4. Discussion

In this study, we utilized satellite-based observations and ground-level measurements at flux towers to demonstrate the widespread occurrence of an afternoon depression in photosynthesis (Figure S2 and Figure S3 in Supporting Information S1). The afternoon depression and peak forward shift in GPP are more pronounced in soil moisture-limited ecosystems with high aridity, which is closely related to moisture availability (Nelson

Figure 2. Disentangling monthly T_{air} and VPD interaction effects from 2000 to 2021. (a) ΔGPP_{SIF} versus VPD, binned by T_{air}. (b) ΔGPP_{SIF} versus T_{air}, binned by VPD. (c) Average ΔGPP_{SIF} in each percentile bin of T_{air} and VPD. (d) Distribution of ΔGPP_{SIF} (VPD|T_{air}) and ΔGPP_{SIF} (T_{air} |VPD). Circles denote ΔGPP(VPD|T_{air}) and ΔGPP(T_{air}|VPD) in each bin, consistent with the legend of (a) and (b). Squares denote the corresponding means. (e, f) Spatial distribution of the changes in ΔGPP_{SIF} caused by high VPD (ΔGPP_{SIF} (VPD|T_{air})) and high T_{air} (ΔGPP_{SIF} (T_{air}|VPD)). (g, h) ΔGPP_{SIF} (VPD|T_{air}) and ΔGPP_{SIF} (T_{air}|VPD) variations across vegetation types and along aridity gradients. ENF, evergreen needleleaf forest; EBF, evergreen broadleaf forest; DNF, deciduous needleleaf forest; DBF, deciduous broadleaf forest; MF, mixed forest; SHR, shrubland; WSA, woody savanna; SAV, savanna; GRA, grassland; CRO, cropland; CNM, cropland/natural vegetation mosaic. The black centerline in each box plot indicates the median, and the bottom and top edges of the box indicate the 25th and 75th percentiles, respectively.

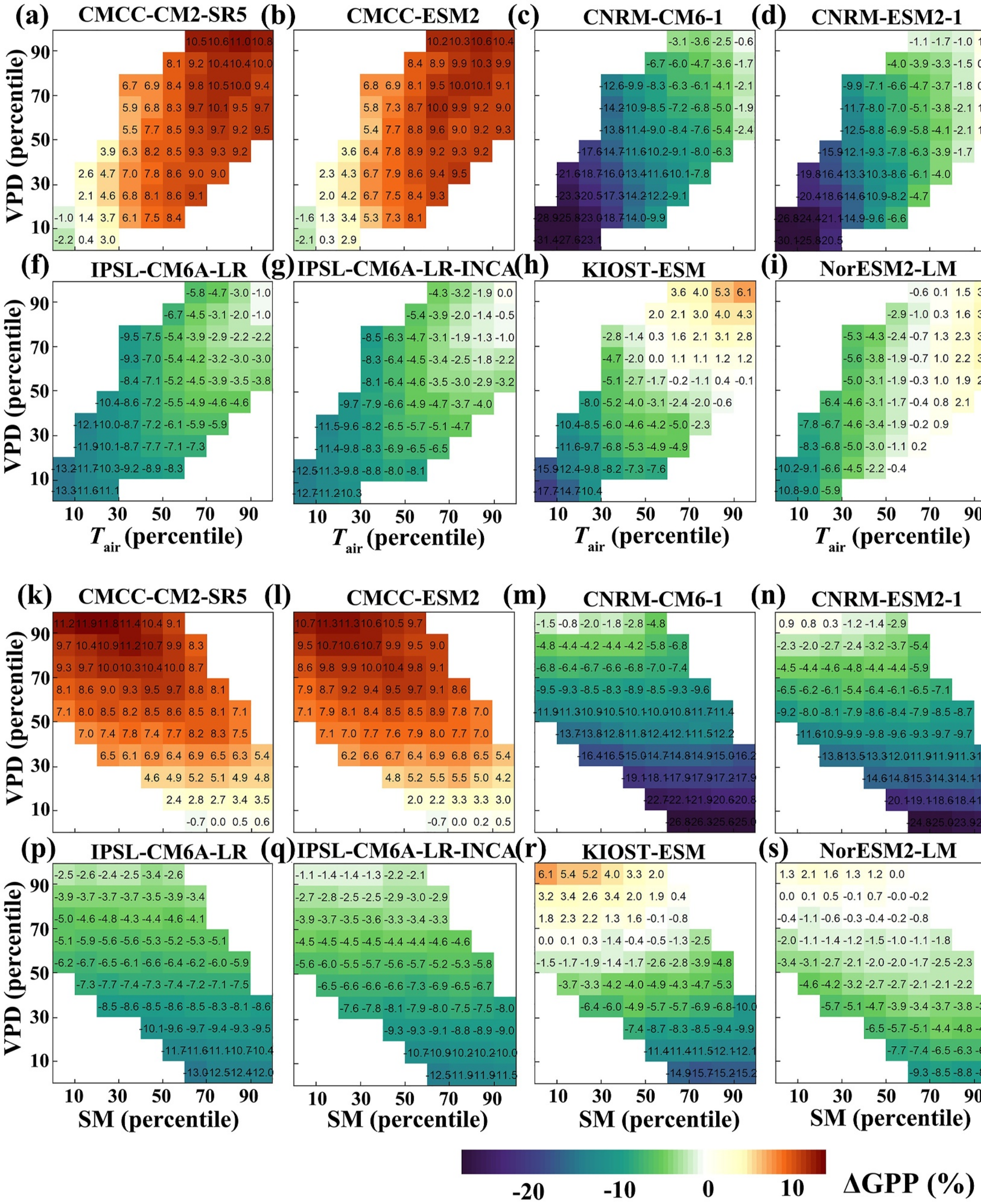

Figure 3. Response of monthly average ΔGPP to monthly VPD, T_{air}, and SM using ten ESMs during 2010–2014. (a–j) Response of ΔGPP to VPD and T_{air}. (k–t) Response of ΔGPP to VPD and SM. The numbers in the figures represent the mean ΔGPP values (ΔGPP = (GPP_{AM}–GPP_{PM}) × 100%/GPP_{AM}) in each percentile bin, with positive values (ΔGPP >0, red) indicating that GPP_{AM} exceeds GPP_{PM}, and negative values (ΔGPP <0, green) indicating that GPP_{PM} exceeds GPP_{AM}.

et al., 2018). Arid regions, characterized by vegetation living in hot and dry conditions (Figure S14 in Supporting Information S1), exhibit heightened sensitivity to climate variability and extremes (Smith et al., 2019). The GPP peak occurs earlier in arid zones than in humid regions, and the peak shifts further toward earlier morning times as soil moisture limitation increases (Figure S6 in Supporting Information S1). In fact, soil moisture controls the pre-dawn leaf water potential, which ultimately controls the stomata sensitivity to VPD (Nelson et al., 2018). Stomata typically close partially in drier air to limit transpiration rate and associated decline in leaf water potential—a response accentuated in dry soil and under drought conditions (Venturas et al., 2017). In arid regions, where soil moisture is limited, plant leaves are more susceptible to water loss under high VPD conditions, leading to earlier stomatal closure and a corresponding advance in the diurnal peak of GPP.

10.1029/2024GL110954

Decoupled analyses of satellite and site observations demonstrate that VPD-induced physiological responses are the primary factors contributing to the decline in afternoon photosynthesis. Due to dewfall, hydraulic lift, or other overnight redistributions of soil moisture, plant stress is typically minimized in the morning (Lambers et al., 2019). Stomatal conductance is generally higher in the morning when VPD is lower, allowing for optimal CO_2 uptake and enhanced photosynthesis. However, as VPD increases throughout the day, plants tend to close their stomata to conserve water (Xu et al., 2020). Notably, higher mean daily VPD is associated with greater increases in afternoon VPD (Figure S15 in Supporting Information S1), which triggers stomatal closure, reduces mesophyll CO_2 concentrations, and decreases afternoon assimilation and light use efficiency (Grossiord et al., 2020; Yuan et al., 2019). This stomatal closure generally occurs more rapidly as VPD rises, resulting in an advance of the GPP peak to earlier in the morning.

Our study reveals that reductions in soil moisture have a weak direct effect on afternoon depression (Figure S9 and Figure S10 in Supporting Information S1). In most global regions, soil moisture indirectly influences afternoon photosynthesis depression through its effect on VPD. However, in tropical regions with significant soil moisture fluctuations (e.g., northern South America and African woody savannas), soil moisture directly affects afternoon photosynthesis depression (Figure S9f in Supporting Information S1). Soil moisture typically has insignificant variation throughout the day, while temperature and VPD show strong daily cycle. Moreover, soil moisture exerts a cumulative effect on carbon assimilation, though its impact is less pronounced on short-term time scales (Green et al., 2019). Notably, our findings reveal that under high soil moisture conditions, the impact of VPD on afternoon photosynthesis depression is mitigated. Sufficient soil moisture maintains high leaf water potentials and low stomatal sensitivity to VPD, allowing plants to sustain high transpiration efficiency even under high afternoon VPD conditions (Zhong et al., 2023). Conversely, low soil moisture reduces leaf-level water potential and xylem water transport, leading to increased stomatal sensitivity to VPD and reduced transpiration (Sperry et al., 2016). This contrast in responses further emphasizes the crucial role of soil water availability in modulating the effects of VPD on plant physiological processes.

Our study advances the understanding of the interplay between temperature and VPD in influencing afternoon photosynthesis depression. We demonstrate that VPD dominates afternoon GPP reductions under water stress, while temperature becomes important under wet conditions. In well-watered regions, a low VPD may not limit stomata conductance and may even promote soil nutrient and CO_2 uptake (Zhong et al., 2023). With VPD remaining constant, an increase in both temperature and absolute humidity may lead to higher rates of photosynthesis in the morning (Zhang, Cescatti, et al., 2023). However, as temperature increases evaporation rates, plants may experience heat stress in the afternoon (e.g., inhibition of biochemical reactions, RuBisCO activity, increased photorespiration rates, and mesophyll conductance) (Dusenge et al., 2019; Lloyd & Farquhar, 2008). Our results emphasize the importance of examining the temporal dynamics of temperature effects on GPP, highlighting potential variations throughout the day.

Based on our findings, VPD plays a pivotal role in governing diurnal carbon dynamics within terrestrial ecosystems. However, most CMIP6 ESMs underestimate VPD's negative effects, resulting in higher afternoon GPP (Figure 3 and Figure S12 in Supporting Information S1). Existing ESMs still poorly assess and simulate the dependence of diurnal GPP variation on VPD variability and associated land-atmosphere feedbacks (Restrepo-Coupe et al., 2017). Most current models only include stomatal limitations on photosynthesis and implement empirical formulations of water-stress functions related to soil moisture content and VPD (Verhoef & Egea, 2014). They have high degrees of uncertainty associated with their representation of canopy conductance, especially in dry environments (Fu et al., 2022). Accounting for surface forcing variables (e.g., VPD) could significantly improve CMIP6 model ensembles (Yuan et al., 2022). Neglecting or underestimating the adverse effects of elevated VPD on afternoon photosynthesis could result in an overestimation of carbon sinks under future climatic conditions. Our results highlight the necessity of implementing improved, mechanistic representations of vegetation responses to VPD stress in ESMs.

Increased soil moisture, typically correlated with higher precipitation and higher cover of convective clouds in the second half of the day, may reduce solar radiation and contribute to the afternoon decline in photosynthesis (Durand et al., 2021; Yue et al., 2024). High VPD, heat stress, and intense solar radiation generally lead to more pronounced afternoon depression of photosynthesis in tropical regions (Fu et al., 2006). In contrast, in high-latitude regions with lower radiation, increased solar radiation enhances photosynthesis. The influence of atmospheric CO_2 concentration on the diurnal cycle was not explicitly considered in our research (e.g., the effect of elevated morning CO_2 due to nocturnal ecosystem respiration). Increased afternoon transpiration may result in lower leaf and surrounding air temperatures, thus reducing VPD. Additionally, even after binned decoupling, the relatively strong correlations between VPD and temperature in high latitudes, and between VPD and soil moisture in the tropics (Figure S1 in Supporting Information S1), may introduce uncertainties into our results. The application of OCO-3 SIF has been limited by its intrinsic spatiotemporal discontinuities (Xiao et al., 2021). The fusion of OCO-3 and geostationary sensors could generate high-resolution spatiotemporal estimates, improving the monitoring of diurnal changes in photosynthesis. Incorporating these factors into future research will provide a more comprehensive understanding of the physiological responses of vegetation to environmental variables.

5. Conclusions

This study utilized satellite and flux towers data to examine the effects of temperature and dryness stress on the diurnal variations of photosynthesis in global terrestrial ecosystems. Our findings reveal that the increase in VPD causes the diurnal centroid of GPP to shift from 12:00 noon to 10:30 a.m., while significant shifts due to temperature are only observed beyond 26°C. After disentangling the interactions between climate factors, we identified VPD as the primary driver of widespread afternoon depression in GPP, particularly in arid regions and areas with short vegetation. ESMs have underestimated the negative impact of VPD on afternoon GPP, leading to a widespread increase in afternoon photosynthesis, with temperature being the key driver. This study highlights the critical role of VPD in the diurnal variations of photosynthesis and underscores the necessity of improving the modeling of VPD effects in ESMs for a more accurate understanding of the global carbon cycle.

Data Availability Statement

OCO-3 SIF can be found in Michael and Annmarie. (2021). Global sub-daily (hourly) GPP_{SIF} data are available at: https://cstr.cn/15732.11.nesdc.ecodb.rs.2024.030. ERA5 monthly averaged data are available at Hersbach et al. (2023). MCD12Q1 land cover is available at M. Friedl and Sulla-Menashe. (2019). Aridity index is available at: https://crudata.uea.ac.uk/cru/data/hrg/cru_ts_4.06. FLUXNET2015 data are available online: under https://fluxnet.org/data/fluxnet2015-dataset/. CMIP6 data are downloaded from: https://esgf-data.dkrz.de/search/cmip6-dkrz/. CMIP6 models used can be found in Table S2 of Supporting Information S1. Leaf area index data are available at Liu et al. (2021).

Acknowledgments
This research was supported by the National Natural Science Foundation of China (42125105), the Natural Science Foundation of Jiangsu Province (BK20240068), the National Natural Science Foundation of China (42471405, 42101320) and the National Key Research and Development Program of China (2022YFF1301900).

References

Beer, C., Reichstein, M., Tomelleri, E., Ciais, P., Jung, M., Carvalhais, N., et al. (2010). Terrestrial gross carbon dioxide uptake: Global distribution and covariation with climate. *Science*, *329*(5993), 834–838. https://doi.org/10.1126/science.1184984

Bucci, S. J., Carbonell Silletta, L. M., Garré, A., Cavallaro, A., Efron, S. T., Arias, N. S., et al. (2019). Functional relationships between hydraulic traits and the timing of diurnal depression of photosynthesis. *Plant, Cell and Environment*, *42*(5), 1603–1614. https://doi.org/10.1111/pce.13512

Chen, Y., Wang, G., & Seth, A. (2024). Climatic drivers for the variation of gross primary productivity across terrestrial ecosystems in the United States. *Journal of Geophysical Research: Biogeosciences*, *129*(8), e2024JG008168. https://doi.org/10.1029/2024JG008168

Ding, Y., Li, Z., & Peng, S. (2020). Global analysis of time-lag and-accumulation effects of climate on vegetation growth. *International Journal of Applied Earth Observation and Geoinformation*, *92*, 102179. https://doi.org/10.1016/j.jag.2020.102179

Durand, M., Murchie, E. H., Lindfors, A. V., Urban, O., Aphalo, P. J., & Robson, T. M. (2021). Diffuse solar radiation and canopy photosynthesis in a changing environment. *Agricultural and Forest Meteorology*, *311*, 108684. https://doi.org/10.1016/j.agrformet.2021.108684

Dusenge, M. E., Duarte, A. G., & Way, D. A. (2019). Plant carbon metabolism and climate change: Elevated CO_2 and temperature impacts on photosynthesis, photorespiration and respiration. *New Phytologist*, *221*(1), 32–49. https://doi.org/10.1111/nph.15283

Friedl, M., & Sulla-Menashe, D. (2019). MCD12Q1 MODIS/Terra+Aqua land cover type yearly L3 global 500m SIN grid V006 [Dataset]. https://doi.org/10.5067/MODIS/MCD12Q1.006

Friedl, M. A., Sulla-Menashe, D., Tan, B., Schneider, A., Ramankutty, N., Sibley, A., & Huang, X. M. (2010). MODIS Collection 5 global land cover: Algorithm refinements and characterization of new datasets. *Remote Sensing of Environment*, *114*(1), 168–182. https://doi.org/10.1016/j.rse.2009.08.016

Fu, Y. L., Yu, G. R., Sun, X. M., Li, Y. N., Wen, X. F., Zhang, L. M., et al. (2006). Depression of net ecosystem CO_2 exchange in semi-arid Leymus chinensis steppe and alpine shrub. *Agricultural and Forest Meteorology*, *137*(3–4), 234–244. https://doi.org/10.1016/j.agrformet.2006.02.009

Fu, Z., Ciais, P., Prentice, I. C., Gentine, P., Makowski, D., Bastos, A., et al. (2022). Atmospheric dryness reduces photosynthesis along a large range of soil water deficits. *Nature Communications*, *13*(1), 989. https://doi.org/10.1038/s41467-022-28652-7

Green, J. K., Seneviratne, S. I., Berg, A. M., Findell, K. L., Hagemann, S., Lawrence, D. M., & Gentine, P. (2019). Large influence of soil moisture on long-term terrestrial carbon uptake. *Nature*, *565*(7740), 476–479. https://doi.org/10.1038/s41586-018-0848-x

Grossiord, C., Buckley, T. N., Cernusak, L. A., Novick, K. A., Poulter, B., Siegwolf, R. T., et al. (2020). Plant responses to rising vapor pressure deficit. *New Phytologist*, *226*(6), 1550–1566. https://doi.org/10.1111/nph.16485

Harris, I., Osborn, T. J., Jones, P., & Lister, D. (2020). Version 4 of the CRU TS monthly high-resolution gridded multivariate climate dataset. *Scientific Data*, *7*(1), 109. https://doi.org/10.1038/s41597-020-0453-3

Hersbach, H., Bell, B., Berrisford, P., Biavati, G., Horányi, A., Muñoz Sabater, J., et al. (2023). ERA5 monthly averaged data on single levels from 1940 to present [Dataset]. *Copernicus Climate Change Service (C3S) Climate Data Store (CDS)*. https://doi.org/10.24381/cds.f17050d7

Hersbach, H., Bell, B., Berrisford, P., Hirahara, S., Horányi, A., Muñoz-Sabater, J., et al. (2020). The ERA5 global reanalysis. *Quarterly Journal of the Royal Meteorological Society*, *146*(730), 1999–2049. https://doi.org/10.1002/qj.3803

Irons, J. R., Dwyer, J. L., & Barsi, J. A. (2012). The next Landsat satellite: The Landsat data continuity mission. *Remote Sensing of Environment*, *122*, 11–21. https://doi.org/10.1016/j.rse.2011.08.026

Khan, A. M., Stoy, P. C., Joiner, J., Baldocchi, D., Verfaillie, J., Chen, M., & Otkin, J. A. (2022). The diurnal dynamics of gross primary productivity using observations from the advanced baseline imager on the geostationary operational environmental satellite-R series at an Oak savanna ecosystem. *Journal of Geophysical Research: Biogeosciences*, *127*(3), e2021JG006701. https://doi.org/10.1029/2021JG006701

Lambers, H., Oliveira, R. S., Lambers, H., & Oliveira, R. S. (2019). Plant water relations. In *Plant Physiological Ecology*. Springer. https://doi.org/10.1007/978-3-030-29639-1_5

Li, X., Ryu, Y., Xiao, J., Dechant, B., Liu, J., Li, B., et al. (2023). New-generation geostationary satellite reveals widespread midday depression in dryland photosynthesis during 2020 western US heatwave. *Science Advances*, *9*(31), eadi0775. https://doi.org/10.1126/sciadv.adi0775

Lin, C., Gentine, P., Frankenberg, C., Zhou, S., Kennedy, D., & Li, X. (2019). Evaluation and mechanism exploration of the diurnal hysteresis of ecosystem fluxes. *Agricultural and Forest Meteorology*, *278*, 107642. https://doi.org/10.1016/j.agrformet.2019.107642

Liu, L., Gudmundsson, L., Hauser, M., Qin, D., Li, S., & Seneviratne, S. (2020). Soil moisture dominates dryness stress on ecosystem production globally. *Nature Communications*, *11*(1), 4892. https://doi.org/10.1038/s41467-020-18631-1

Liu, R., Liu, Y., & Chen, J. (2021). GLOBMAP global leaf area index since 1981 (version 3.0) [Dataset]. *Zenodo*. https://doi.org/10.5281/zenodo.4700264

Liu, Y., Liu, R., & Chen, J. M. (2012). Retrospective retrieval of long-term consistent global leaf area index (1981–2011) from combined AVHRR and MODIS data. *Journal of Geophysical Research*, *117*(G4), G04003. https://doi.org/10.1029/2012JG002084

Lloyd, J., & Farquhar, G. D. (2008). Effects of rising temperatures and [CO_2] on the physiology of tropical forest trees. *Philosophical Transactions of the Royal Society B: Biological Sciences*, *363*(1498), 1811–1817. https://doi.org/10.1098/rstb.2007.0032

Michael, G., & Annmarie, E. (2021). OCO-3 Level 2 bias-corrected solar-induced fluorescence and other select fields from the IMAP-DOAS algorithm aggregated as daily files, Retrospective processing V10r [Dataset]. Goddard Earth Sciences Data and Information Services Center (GES DISC). https://doi.org/10.5067/NOD1DPPBCXSO

Nelson, J. A., Carvalhais, N., Migliavacca, M., Reichstein, M., & Jung, M. (2018). Water-stress-induced breakdown of carbon–water relations: Indicators from diurnal FLUXNET patterns. *Biogeosciences*, *15*(8), 2433–2447. https://doi.org/10.5194/bg-15-2433-2018

Pastorello, G., Trotta, C., Canfora, E., Chu, H., Christianson, D., Cheah, Y.-W., et al. (2020). The FLUXNET2015 dataset and the ONEFlux processing pipeline for eddy covariance data. *Scientific Data*, *7*(1), 1–27. https://doi.org/10.1038/s41597-021-00851-9

Restrepo-Coupe, N., Levine, N. M., Christoffersen, B. O., Albert, L. P., Wu, J., Costa, M. H., et al. (2017). Do dynamic global vegetation models capture the seasonality of carbon fluxes in the Amazon basin? A data-model intercomparison. *Global Change Biology*, *23*(1), 191–208. https://doi.org/10.1111/gcb.13442

Smith, W. K., Dannenberg, M. P., Yan, D., Herrmann, S., Barnes, M. L., Barron-Gafford, G. A., et al. (2019). Remote sensing of dryland ecosystem structure and function: Progress, challenges, and opportunities. *Remote Sensing of Environment*, *233*, 111401. https://doi.org/10.1016/j.rse.2019.111401

Sperry, J. S., Wang, Y., Wolfe, B. T., Mackay, D. S., Anderegg, W. R., McDowell, N. G., & Pockman, W. T. (2016). Pragmatic hydraulic theory predicts stomatal responses to climatic water deficits. *New Phytologist*, *212*(3), 577–589. https://doi.org/10.1111/nph.14059

Sun, Y., Frankenberg, C., Wood, J. D., Schimel, D. S., Jung, M., Guanter, L., et al. (2017). OCO-2 advances photosynthesis observation from space via solar-induced chlorophyll fluorescence. *Science*, *358*(6360), eaam5747. https://doi.org/10.1126/science.aam5747

Taylor, T. E., Eldering, A., Merrelli, A., Kiel, M., Somkuti, P., Cheng, C., et al. (2020). OCO-3 early mission operations and initial (vEarly) XCO_2 and SIF retrievals. *Remote Sensing of Environment*, *251*, 112032. https://doi.org/10.1016/j.rse.2020.112032

Venturas, M. D., Sperry, J. S., & Hacke, U. G. (2017). Plant xylem hydraulics: What we understand, current research, and future challenges. *Journal of Integrative Plant Biology*, *59*(6), 356–389. https://doi.org/10.1111/jipb.12534

Verhoef, A., & Egea, G. (2014). Modeling plant transpiration under limited soil water: Comparison of different plant and soil hydraulic parameterizations and preliminary implications for their use in land surface models. *Agricultural and Forest Meteorology*, *191*, 22–32. https://doi.org/10.1016/j.agrformet.2014.02.009

Will, R. E., Wilson, S. M., Zou, C. B., & Hennessey, T. C. (2013). Increased vapor pressure deficit due to higher temperature leads to greater transpiration and faster mortality during drought for tree seedlings common to the forest–grassland ecotone. *New Phytologist*, *200*(2), 366–374. https://doi.org/10.1111/nph.12321

Wilson, K. B., Baldocchi, D., Falge, E., Aubinet, M., Berbigier, P., Bernhofer, C., et al. (2003). Diurnal centroid of ecosystem energy and carbon fluxes at FLUXNET sites. *Journal of Geophysical Research*, *108*(D21), 4664. https://doi.org/10.1029/2001JD001349

Wu, J., Guan, K., Hayek, M., Restrepo-Coupe, N., Wiedemann, K. T., Xu, X., et al. (2017). Partitioning controls on Amazon forest photosynthesis between environmental and biotic factors at hourly to interannual timescales. *Global Change Biology*, *23*(3), 1240–1257. https://doi.org/10.1111/gcb.13509

Xiao, J., Fisher, J. B., Hashimoto, H., Ichii, K., & Parazoo, N. C. (2021). Emerging satellite observations for diurnal cycling of ecosystem processes. *Nature Plants*, *7*(7), 877–887. https://doi.org/10.1038/s41477-021-00952-8

Xu, H., Xiao, J., & Zhang, Z. (2020). Heatwave effects on gross primary production of northern mid-latitude ecosystems. *Environmental Research Letters*, *15*(7), 074027. https://doi.org/10.1088/1748-9326/ab8760

Yuan, K., Zhu, Q., Riley, W. J., Li, F., & Wu, H. (2022). Understanding and reducing the uncertainties of land surface energy flux partitioning within CMIP6 land models. *Agricultural and Forest Meteorology*, *319*, 108920. https://doi.org/10.1016/j.agrformet.2022.108920

Yuan, W., Zheng, Y., Piao, S., Ciais, P., Lombardozzi, D., Wang, Y., et al. (2019). Increased atmospheric vapor pressure deficit reduces global vegetation growth. *Science Advances*, *5*(8), eaax1396. https://doi.org/10.1126/sciadv.aax1396

Yue, J., Li, T., Feng, H., Fu, Y., Liu, Y., Tian, J., et al. (2024). Enhancing field soil moisture content monitoring using laboratory-based soil spectral measurements and radiative transfer models. *Agriculture Communications*, *2*(4), 100060. https://doi.org/10.1016/j.agrcom.2024.100060

Zhang, Y., Cai, M., Xiao, X., Yang, X., Migliavacca, M., Basara, J., et al. (2024). Immediate and lagged vegetation responses to dry spells revealed by continuous solar-induced chlorophyll fluorescence observations in a tall-grass prairie. *Remote Sensing of Environment*, *305*, 114080. https://doi.org/10.1016/j.rse.2024.114080

Zhang, Y., Song, C., Band, L. E., Sun, G., & Li, J. (2017). Reanalysis of global terrestrial vegetation trends from MODIS products: Browning or greening? *Remote Sensing of Environment*, *191*, 145–155. https://doi.org/10.1016/j.rse.2016.12.018

Zhang, Y., Xiao, X., Zhang, Y., Wolf, S., Zhou, S., Joiner, J., et al. (2018). On the relationship between sub-daily instantaneous and daily total gross primary production: Implications for interpreting satellite-based SIF retrievals. *Remote Sensing of Environment*, *205*, 276–289. https://doi.org/10.1016/j.rse.2017.12.009

Zhang, Z., Cescatti, A., Wang, Y. P., Gentine, P., Xiao, J., Guanter, L., et al. (2023). Large diurnal compensatory effects mitigate the response of Amazonian forests to atmospheric warming and drying. *Science Advances*, *9*(21), eabq4974. https://doi.org/10.1126/sciadv.abq4974

Zhang, Z., Guanter, L., Porcar-Castell, A., Rossini, M., Pacheco-Labrador, J., & Zhang, Y. (2023). Global modeling diurnal gross primary production from OCO-3 solar-induced chlorophyll fluorescence. *Remote Sensing of Environment*, *285*, 113383. https://doi.org/10.1016/j.rse.2022.113383

Zhang, Z., Zhang, Y., Porcar-Castell, A., Joiner, J., Guanter, L., Yang, X., et al. (2020). Reduction of structural impacts and distinction of photosynthetic pathways in a global estimation of GPP from space-borne solar-induced chlorophyll fluorescence. *Remote Sensing of Environment*, *240*, 111722. https://doi.org/10.1016/j.rse.2020.111722

Zhong, Z., He, B., Wang, Y.-P., Chen, H. W., Chen, D., Fu, Y. H., et al. (2023). Disentangling the effects of vapor pressure deficit on northern terrestrial vegetation productivity. *Science Advances*, *9*(32), eadf3166. https://doi.org/10.1126/sciadv.adf3166

References From the Supporting Information

Bentsen, M., Oliviè, D. J. L., Seland, Ø., Toniazzo, T., Gjermundsen, A., Graff, L. S., et al. (2019). NCC NorESM2-MM model output prepared for CMIP6 CMIP historical [Dataset]. *Earth System Grid Federation*. https://doi.org/10.22033/ESGF/CMIP6.8040

Boucher, O., Denvil, S., Levavasseur, G., Cozic, A., Caubel, A., Foujols, M.-A., et al. (2021). IPSL IPSL-CM6A-LR-INCA model output prepared for CMIP6 CMIP [Dataset]. *Earth System Grid Federation*. https://doi.org/10.22033/ESGF/CMIP6.13582

Boucher, O., Servonnat, J., Albright, A. L., Aumont, O., Balkanski, Y., Bastrikov, V., et al. (2020). Presentation and evaluation of the IPSL-CM6A-LR climate model. *Journal of Advances in Modeling Earth Systems*, *12*(7), e2019MS002010. https://doi.org/10.1029/2019MS002010

Breiman, L. (2001). Random forests. *Machine Learning*, *45*(1), 5–32. https://doi.org/10.1023/A:1010933404324

Fogli, P. G., Iovino, D., & Lovato, T. (2020). CMCC CMCC-CM2-SR5 model output prepared for CMIP6 OMIP omip1 [Dataset]. *Earth System Grid Federation*. https://doi.org/10.22033/ESGF/CMIP6.13230

Kim, Y., Noh, Y., Kim, D., Lee, M.-I., Lee, H. J., Kim, S. Y., & Kim, D. (2019). KIOST KIOST-ESM model output prepared for CMIP6 CMIP [Dataset]. *Earth System Grid Federation*. https://doi.org/10.22033/ESGF/CMIP6.1922

Knauer, J., Zaehle, S., Medlyn, B. E., Reichstein, M., Williams, C. A., Migliavacca, M., et al. (2018). Towards physiologically meaningful water-use efficiency estimates from eddy covariance data. *Global Change Biology*, *24*(2), 694–710. https://doi.org/10.1111/gcb.15535

Lovato, T., Peano, D., & Butenschön, M. (2021). CMCC CMCC-ESM2 model output prepared for CMIP6 CMIP historica l [Dataset]. *Earth System Grid Federation*. https://doi.org/10.22033/ESGF/CMIP6

Roberts, M. (2017). MOHC HadGEM3-GC31-LL model output prepared for CMIP6 HighResMIP [Dataset]. *Earth System Grid Federation*. https://doi.org/10.22033/ESGF/CMIP6.1901

Séférian, R., Nabat, P., Michou, M., Saint-Martin, D., Voldoire, A., Colin, J., et al. (2019). Evaluation of CNRM Earth system model, CNRM-ESM2-1: Role of Earth system processes in present-day and future climate. *Journal of Advances in Modeling Earth Systems*, *11*(12), 4182–4227. https://doi.org/10.1029/2019MS001791

Seland, Ø., Bentsen, M., Oliviè, D. J. L., Toniazzo, T., Gjermundsen, A., Graff, L. S., et al. (2019). NCC NorESM2-LM model output prepared for CMIP6 CMIP historical [Dataset]. *Earth System Grid Federation*. https://doi.org/10.22033/ESGF/CMIP6.8036

Voldoire, A., Saint-Martin, D., Sénési, S., Decharme, B., Alias, A., Chevallier, M., et al. (2019). Evaluation of CMIP6 deck experiments with CNRM-CM6-1. *Journal of Advances in Modeling Earth Systems*, *11*(7), 2177–2213. https://doi.org/10.1029/2019MS001683